Low-temperature heat capacities and Raman spectra of negative thermal expansion compounds ZrW_2O_8 and HfW_2O_8

Yasuhisa Yamamura, Noriyuki Nakajima, Toshihide Tsuji,* Mikio Koyano, Yoshihiro Iwasa,† and Shin'ichi Katayama
Center for New Materials and School of Materials Science, Japan Advanced Institute of Science and Technology, 1-1 Asahidai, Tatsunokuchi, Ishikawa 923-1292, Japan

Kazuya Saito and Michio Sorai
Research Center for Molecular Thermodynamics, Graduate School of Science, Osaka University, Toyonaka, Osaka 560-0043, Japan
(Received 6 December 2001; published 20 June 2002)

Heat capacities of ZrW_2O_8 and HfW_2O_8 were precisely measured between 1.8 and 330 K. Heat-capacity curves of ZrW_2O_8 and HfW_2O_8 are very similar to each other. The heat capacity of HfW_2O_8 at low temperature is larger than that of ZrW_2O_8 due to atomic mass effect, but both heat capacities cross around 220 K. Raman spectra of ZrW_2O_8 and HfW_2O_8 were recorded at room temperature. Frequency distributions of lattice vibrations were estimated through an analysis of the heat capacities for ZrW_2O_8 and HfW_2O_8. It is found that the difference in the frequency distributions between ZrW_2O_8 and HfW_2O_8 arises from the different atomic mass and bond strength, and causes the different temperature dependence of the heat capacities. The properties of the optical-phonon modes with a large negative mode-Grüneisen parameter are discussed.

DOI: 10.1103/PhysRevB.66.014301 PACS number(s): 63.20.−e, 65.40.−b, 78.30.Hv

I. INTRODUCTION

Most materials expand with increasing temperature, because of the increase in distance between the constituting particles that vibrate in an anharmonic potential. There are, however, some materials that contract with increasing temperature. One of them is ZrW_2O_8, which has recently received considerable attention. ZrW_2O_8 contracts isotropically in a very wide temperature range from 0.3 to 1050 K.[1–3] The crystal structure of ZrW_2O_8 is very rare and consists of ZrO_6 octahedra and WO_4 tetrahedra. Those polyhedra share the oxygen atoms at the vertexes of the polyhedra next to each other except one of the oxygen atoms of a WO_4 unit, which is called a ''terminal oxygen.''

It is widely accepted that the vibrations of the ZrO_6 and WO_4 polyhedra cause the negative thermal expansion of ZrW_2O_8.[4] Both ZrO_6 and WO_4 units have very hard metal-oxygen bonds Zr-O and W-O, which cause transverse vibrational modes of oxygen atoms perpendicular to the bond axis of the W-O-Zr bridge, leading to low-energy librational and translational modes of the undistorted ZrO_6 and WO_4 polyhedra.[4] Many of the previous studies (inelastic neutron scattering,[5,6] heat capacity,[7] analysis of thermal expansion,[8,9] and lattice-dynamic calculation[10,11]) have suggested that a family of the vibrational modes with large negative mode-Grüneisen parameters is in the energy region from 1.5 to 8.5 meV and dominates the overall negative thermal-expansion properties of ZrW_2O_8.

The low-energy vibrations of the undistorted polyhedra strongly depend on a kind of cation at the center of the polyhedra, because a center cation determines the atomic mass and the size of the polyhedra. This suggests that the AB_2O_8 type materials with another center cation possibly have different lattice vibration from ZrW_2O_8. Hafnium tungsten oxide (HfW_2O_8) having a Hf^{4+} cation at the center of octahedra has the same crystal structure as ZrW_2O_8,[1,2,12] and shows the negative thermal expansion similarly to ZrW_2O_8.[12,13] It is well known that zirconium and hafnium ions resemble each other in chemical properties, in spite of a large difference in the atomic number of 32. The two elements have nearly the same ionic radius because of lanthanoid contraction for hafnium:[14] An ionic radius of Zr^{4+} with sixfold coordination is 86 pm and that of Hf^{4+} is 85 pm.[15] However the atomic mass of hafnium (178.5) is about twice heavier than that of zirconium (91.2). It is, thus, expected that the large difference in atomic mass leads to different lattice vibrations between ZrW_2O_8 and HfW_2O_8. Indeed, the mass effect is reflected in heat capacities of ZrO_2 and HfO_2. At room temperature, the heat capacity of HfO_2 (60 J K^{-1} mol^{-1}) (Ref. 16) is larger than that of ZrO_2 (56 J K^{-1} mol^{-1}) (Ref. 16) due to the mass effect. We have reported the accurate heat-capacity data for HfW_2O_8 below 330 K and ZrW_2O_8 from 300 to 330 K in previous short communications.[17,18] In contrast to the expected mass effect, the heat capacity of HfW_2O_8 was somewhat smaller than that of ZrW_2O_8 (Ref. 17) at room temperature. Considering the mass effect on heat capacity, it is expected that the two heat-capacity curves of ZrW_2O_8 and HfW_2O_8 have an intersection below room temperature.[17] In order to confirm the intersection, accurate heat-capacity data for ZrW_2O_8 below room temperature are needed.

It is also expected that the mass effect affects the difference in negative thermal expansion between ZrW_2O_8 and HfW_2O_8, because the negative thermal expansions of these compounds originate from lattice vibrations.[4] To clarify the mass effect of the central cation on lattice vibration, we carried out heat-capacity and Raman spectroscopic experiments for ZrW_2O_8 and HfW_2O_8. Raman spectroscopy is very a popular and useful method to study phonon properties of crystals. However, all information about lattice vibration cannot be obtained by Raman or infrared spectroscopies only, because the spectroscopic experiments have observa-

tional restriction due to selection rule and give no information except for the Γ point in the Brillouin zone. On the other hand, calorimetry can exclude these problems. Moreover, heat capacity gives a lot of information on phonon properties, since heat capacity reflects the phonon density of states. Hitherto there have been a lot of studies on phonon properties by using heat-capacity measurements.[7,19–22] Combining spectroscopy with calorimetry, therefore, is very useful to study phonon properties of materials. In this study, phonon properties of ZrW_2O_8 and HfW_2O_8 are investigated by Raman spectra and phonon densities of states of both compounds are obtained from an analysis of the measured heat-capacity data.

II. EXPERIMENT

ZrW_2O_8 and HfW_2O_8 were prepared by a conventional solid-state reaction as described previously.[13,17,18] Heat-capacity measurements of the sintered samples were carried out from 1.8 to 330 K by using two calorimeters. One was a laboratory-made adiabatic calorimeter for the temperature region above 10 K. The apparatus and operation of the adiabatic calorimeter were described elsewhere.[23] Each sample was loaded into the calorimeter vessel and sealed with He gas (8 kPa at room temperature) to assist quick thermal equilibration in the vessel. The contribution of the helium gas to the total heat capacity was negligibly small. The masses of the ZrW_2O_8 and HfW_2O_8 samples loaded into the vessel were 13.2571 g (0.022 588 mol) and 17.9646 g (0.026 647 mol), respectively, after buoyancy correction. Each sample contributed more than 20% at all temperatures to the total heat capacity including that of the calorimeter vessel. A platinum resistance thermometer (S1055, Minco Products, Inc.) from 13.8 to 330 K and a germanium resistance thermometer (GR-200B-500, Lake-Shore Cryotronics, Inc.) from 4.2 to 13.8 K were used for thermometry. Their temperature scales are based on the ITS-90. The other apparatus used for calorimetry was a commercial relaxation calorimeter (Quantum Design PPMS) for the temperature region below 20 K. ZrW_2O_8 and HfW_2O_8 of 11.345 mg and 13.445 mg, respectively, were weighed, and each sample was contacted to the sample holder with Apiezon-N grease. Raman spectra of ZrW_2O_8 and HfW_2O_8 from 32 to 1200 cm^{-1} were recorded at room temperature using a Jobin Yvon T64000 Raman spectrometer with excitation by an argon-ion laser (514.5 nm and 100 mW).

III. RESULTS

A. Heat capacity

Heat capacities of ZrW_2O_8 and HfW_2O_8 measured from 1.8 to 330 K are plotted in Fig. 1, where the previous heat-capacity data of ZrW_2O_8 below 330 K reported by Ramirez and Kowach[7] are shown as the broken curve for the comparison. The heat-capacity data of ZrW_2O_8 by Ramirez and Kowach[7] are obviously larger than those of ZrW_2O_8 by the present authors. The heat capacity of ZrW_2O_8 at room temperature obtained in this study is about 200 J K^{-1} mol^{-1}, which is about 10% smaller than that of Ramirez and Kowach (220 J K^{-1} mol^{-1}).[7] Judging from inaccuracy ($\pm 0.5\%$) and imprecision ($\pm 0.05\%$) of the present adiabatic calorimeter,[23] it is very likely that Ramirez and Kowach[7] overestimated the heat capacity of ZrW_2O_8. Indeed, Ernst *et al.*[5] pointed out that the heat capacity at room temperature estimated from the phonon density of states, which was obtained from the inelastic neutron-scattering study, was about 10% smaller than their experimental heat-capacity data.

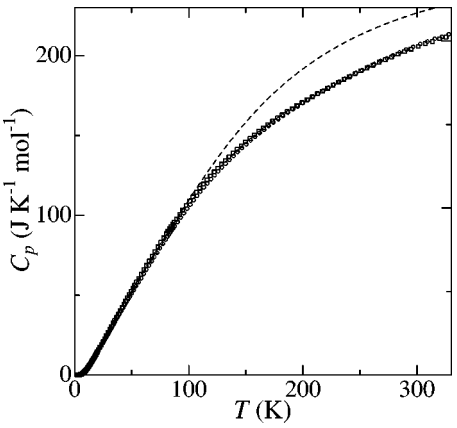

FIG. 1. Measured molar heat capacities of ZrW_2O_8 (circles) and HfW_2O_8 (squares) in this study. The broken line is the heat capacity of ZrW_2O_8 reported by Ramirez and Kowach (Ref. 7).

As seen in Fig. 1, temperature dependence of the heat capacity of HfW_2O_8 is quite similar to that of ZrW_2O_8 in this study. There is no anomaly below room temperature. A close inspection reveals an interesting fact that the heat capacities of ZrW_2O_8 and HfW_2O_8 cross around 220 K. To see the details, the heat capacity of ZrW_2O_8 was subtracted from that of HfW_2O_8, and the difference ΔC_p $[=C_p(HfW_2O_8)\text{-}C_p(ZrW_2O_8)]$ is plotted against temperature in Fig. 2. The ΔC_p is positive at low temperatures, but negative at high temperatures. In accordance with the mass effect, the heat capacity of HfW_2O_8 with heavier formula mass is larger than that of ZrW_2O_8 with lighter formula mass at low temperatures. The ΔC_p gives rise to a maximum around 80 K and decreases with increasing temperature. Since there are no degrees of freedom other than motional

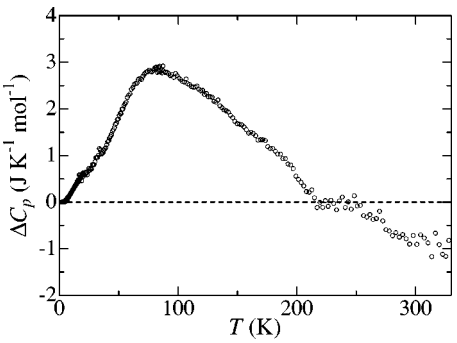

FIG. 2. Difference in heat capacity (C_p) between HfW_2O_8 and ZrW_2O_8, $\Delta C_p = C_p(HfW_2O_8)\text{-}C_p(ZrW_2O_8)$.

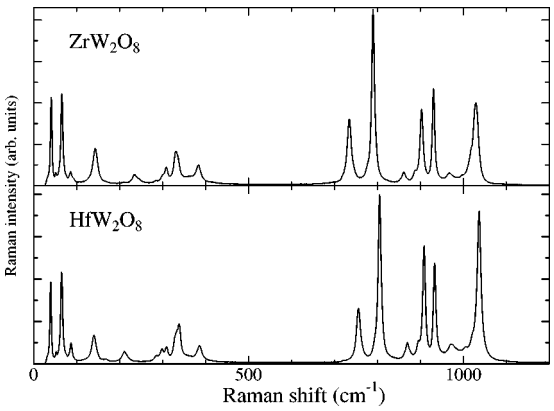

FIG. 3. Raman spectra of ZrW_2O_8 and HfW_2O_8 at room temperature.

ones in both materials, this peculiar behavior should be attributed to the ''lattice'' properties of ZrW_2O_8 and/or HfW_2O_8.

B. Raman spectroscopy

Figure 3 shows the Raman spectra of ZrW_2O_8 and HfW_2O_8 at room temperature. The spectrum of ZrW_2O_8 in this study coincides well with those of two previous works.[2,24] The Raman spectrum for HfW_2O_8 is reported for the first time here.

Raman spectra of HfW_2O_8 and ZrW_2O_8 are very similar and all lines are easily correlated with each other, as both compounds have the same crystal structure. The recorded Raman spectra of each compound consist of two groups, low- and high-frequency lines. There is a wide gap between them. The wide gap suggests the absence of optical-phonon modes at the Γ point, since all the optical-phonon modes of ZrW_2O_8 and HfW_2O_8 are Raman active according to a factor group analysis. The gap of HfW_2O_8 is wider than that of ZrW_2O_8 as seen in Fig. 3. This is mainly due to the shift of the high-frequency group of HfW_2O_8 toward the higher-frequency side (hardening), compared to that of ZrW_2O_8.

Raman shifts of ZrW_2O_8 and HfW_2O_8 are summarized in Table I. Although good correspondence is found between ZrW_2O_8 and HfW_2O_8, most lines are slightly shifted to higher or lower frequency. For example, the peak at 235 cm^{-1} (29.1 meV) for ZrW_2O_8 moves drastically to 211 cm^{-1} (26.2 meV) for HfW_2O_8. The third column in Table I indicates the direction of the shift, on going from ZrW_2O_8 to HfW_2O_8: ''H'' for hardening (shift to high frequency) and ''S'' for softening (shift to low frequency). The fourth column in Table I shows the reported mode-Grüneisen parameters by Raman study under pressure,[24] which will be discussed later.

Considering the crystal structure consisting of two polyhedra, the high-frequency group is attributed to the intrapolyhedra vibrations, whereas the low-frequency group to translational and librational modes of semirigid polyhedra. As shown in Table I, all lines belonging to the high-frequency group bear the symbol ''H,'' indicating hardening, on going from ZrW_2O_8 to HfW_2O_8. On the other hand, the lines belonging to the low-frequency group show both hardening and softening.

TABLE I. Raman data of ZrW_2O_8 and HfW_2O_8 at room temperature.

ZrW_2O_8 Raman shift (cm^{-1})	HfW_2O_8 Raman shift (cm^{-1})	Softening (S) or hardening (H) [a]	Mode-Grüneisen parameter for ZrW_2O_8 [b]
40.9	39.5	S	-1.29
51.7	52.6	H	
65.8	65.3	S	2.51
75.6	75.5		-2.25
86.2	87.1	H	-4.66
143	140	S	-2.21
235	211	S	0.12
245			-1.6
284	286	H	
300	299	S	
308	309	H	-2.24
331			
334	338	H	-0.17
384	386	H	-1.12
735	756	H	0.08
744	764	H	0.82
774	790	H	-0.1
790	805	H	0.28
862	870	H	0.87
888	896	H	-0.05
903	909	H	0.32
931	933	H	0.13
967	972	H	-0.6
996	1005	H	
1019	1022	H	0.23
1029	1037	H	2.2

[a]Direction of the Raman shift, on going from ZrW_2O_8 to HfW_2O_8.
[b]From Ref. 24.

IV. DATA ANALYSIS AND DISCUSSION

A. Debye temperature and bond strength

Figure 4 shows the heat capacities of ZrW_2O_8 and HfW_2O_8 plotted as C_pT^{-1} vs T^2 in a very low-temperature region. The absolute value of heat-capacity of HfW_2O_8 is larger than that of ZrW_2O_8 in the temperature region as seen in Fig. 4. The broken and solid lines in Fig. 4 were determined from the heat capacity data of HfW_2O_8 and ZrW_2O_8, respectively, in the narrow temperature range 1.8 – 2.6 K using a linear least-squares method. These lines mean that the heat capacity of each compound is proportional to T^3 and obeys the Debye T^3 law in this limited temperature region. The slopes in Fig. 4 correspond to the mean sound velocities averaged over propagating direction $\langle v^{-3}\rangle^{-1/3} = 2708$ m s^{-1} and 2666 m s^{-1} for ZrW_2O_8 and HfW_2O_8,

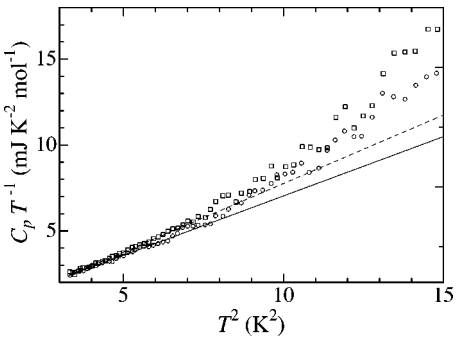

FIG. 4. C_pT^{-1} vs T^2 plots of ZrW_2O_8 (circles) and HfW_2O_8 (squares). The solid (ZrW_2O_8) and broken (HfW_2O_8) lines show the Debye T^3 law.

respectively. The mean sound velocity is expressed by the relation, $3\langle v^{-3}\rangle = \langle v_l^{-3}\rangle + 2\langle v_t^{-3}\rangle$, where v_l and v_t are sound velocities of longitudinal and transverse waves, respectively. The Debye temperatures (Θ_D) of ZrW_2O_8 and HfW_2O_8 are estimated as 311 and 307 K, respectively, from the slopes in Fig. 4, assuming 33 degrees of freedom per formula unit.

The Debye theory of lattice heat capacity takes into account only the acoustic modes of lattice vibrations while solids are treated as an elastic continuum. In this treatment, the Debye temperature depends only on the sound velocity, which is determined by bulk elastic constant and mass density. Since the lattice parameters of ZrW_2O_8 ($a = 0.916$ nm) (Ref. 13) and HfW_2O_8 ($a = 0.913$ nm) (Ref. 13) at room temperature are nearly the same values, the density is proportional to formula mass (586.9 g mol^{-1} for ZrW_2O_8 and 674.2 g mol^{-1} for HfW_2O_8). Then from the experimental Θ_D, the ratio of the (averaged) bond strength for HfW_2O_8 to that for ZrW_2O_8 can be deduced as $[\Theta_D(ZrW_2O_8)/\Theta_D(HfW_2O_8)]^2 \sim (674/587) \approx 1.15$. Namely, the bond in HfW_2O_8 is 1.15 times stronger than that in ZrW_2O_8, in terms of force constant. This increased bond strength is responsible for the hardening of the high-frequency intrapolyhedra vibrations observed in the Raman spectra as summarized in the third column of Table I, because interpolyhedra coupling via the bond linking them surely contributes positively to frequencies.

The heat capacities of ZrW_2O_8 and HfW_2O_8 above about 2.8 K deviate from the solid and broken straight lines, respectively. It is known that the T^3 law practically holds below about $\Theta_D/50$. The deviation from the T^3 law above 2.8 K implies that the above estimate of the Debye temperatures is not adequate for the present cases. This inadequacy may be related to the assumed degrees of freedom. For example, the Θ_D values are calculated as 140 K for ZrW_2O_8 and 138 K for HfW_2O_8 by assuming three degrees of freedom per formula unit. These estimated values are certainly more consistent because the $\Theta_D/50$ values of both crystals give about 3 K as the upper temperature limit of applicability of the T^3 law.

B. Effective phonon density of states of ZrW_2O_8

The C_pT^{-3} of both ZrW_2O_8 and HfW_2O_8 are plotted against $\log T$ in Fig. 5. Both ZrW_2O_8 (circles) and HfW_2O_8 (squares) show a constant C_pT^{-3} in the narrow temperature range below 2.6 K and a large peak at about 9.5 K. This plot gives us fruitful information on the various contributions of vibrational modes to heat capacity. The heat capacities of ZrW_2O_8 and HfW_2O_8 calculated from the Debye temperature using the Debye function are represented as solid and broken curves, respectively, in Fig. 5. Those curves represent Debye contributions, of which C_pT^{-3} is constant at small T and then decreases gently with increasing T. On the other hand, optical-phonon modes approximated well by the Einstein model give a peak. In the case of ZrW_2O_8, it is reported[7] that the peak is due to low-energy Einstein modes. HfW_2O_8 has the similar peak to ZrW_2O_8, so it is natural to say that the low-energy Einstein modes for HfW_2O_8 also contribute to heat capacity. Although the peak of HfW_2O_8 is located at nearly the same temperature as that of ZrW_2O_8, the height and width of the peak for HfW_2O_8 are remarkably larger than those of ZrW_2O_8. This suggests that a distribution of low-energy optical-phonon modes in HfW_2O_8 is different from that in ZrW_2O_8. To compare vibration modes of HfW_2O_8 with those of ZrW_2O_8, we now try to deduce the phonon density of states (DOS) from the heat capacities for ZrW_2O_8 and HfW_2O_8. The adequacy of the deduced effective DOS may be assessed by the comparison with the experimental Raman spectra and the reproduction of the crossing of heat capacity seen in Fig. 1.

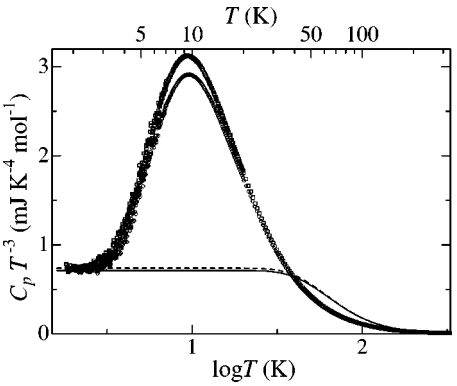

FIG. 5. C_pT^{-3} against $\log T$ for ZrW_2O_8 (circles) and HfW_2O_8 (squares). The solid (ZrW_2O_8) and broken (HfW_2O_8) curves are Debye functions with the Debye temperature 311 and 307 K, respectively, assuming 33 degrees of freedom per formula unit.

The heat capacity of crystal is represented as the sum of C_i, which is the contribution of each vibrational mode i to the heat capacity. Namely, the heat capacity of all lattice vibrations $C_{\rm vib}$ is related to the phonon DOS, $g(\omega)$ $[\int_0^\infty g(\omega)d\omega = 1]$, as follows:

$$C_{\rm vib} = 3rN_A k_B \int_0^\infty \frac{(\hbar\omega/k_BT)^2 \exp(\hbar\omega/k_BT) g(\omega)}{[\exp(\hbar\omega/k_BT)-1]^2} d\omega, \tag{1}$$

where N_A is the Avogadro constant, r the number of atoms per chemical formula, $3rN_A$ the number of degrees of freedom per 1 mol, k_B the Boltzmann constant, $\hbar$ the Dirac constant, and ω the vibration frequency. The above equation, in principle, enables us to estimate the phonon DOS for the

crystal from the experimental heat capacity as a function of temperature. Unfortunately, the precision and accuracy of calorimetry of the present day are insufficient to convert directly measured heat capacity to the phonon DOS. For such purposes, one to two more significant digit(s) (i.e., inaccuracy of 10 – 100 ppm) are necessary. Some simplifications are, consequently, required to solve this problem. Ramirez and Kowach[7] described the heat capacity of ZrW_2O_8 with two Debye and two Einstein functions analytically. In their method, the Debye function with high characteristic temperature compensates for most of the heat capacity of the crystal. Although Ramirez and Kowach[7] succeeded in detecting characteristic low-frequency Einstein modes, it was difficult to express a complex frequency distribution of lattice vibrations only by the two kinds of function. Besides, this method is unsuitable to discuss the frequency distribution in a high-frequency region.

Considering the broad distribution over a rather wide frequency range reported by a neutron inelastic-scattering study,[5] we introduce here a rectangular distribution (see Fig. 7 below). Namely, g_{const} is constant, independently of ω in the frequency range from ω_{L} to ω_{H}. This rectangular frequency distribution of lattice vibrations is related to the heat-capacity contribution C_{R} by the following equation,

$$C_{\mathrm{R}} = nN_{\mathrm{A}}k_{\mathrm{B}}g_{\mathrm{const}}\int_{\omega_{\mathrm{L}}}^{\omega_{\mathrm{H}}}\frac{(\hbar\omega/k_{\mathrm{B}}T)^2\exp(\hbar\omega/k_{\mathrm{B}}T)}{[\exp(\hbar\omega/k_{\mathrm{B}}T)-1]^2}d\omega, \quad (2)$$

where n is the number of degrees of freedom included in the distribution. This equation describes a wide and continuous frequency distribution of lattice vibrations by a single function with three parameters (g_{const}, ω_{L}, and ω_{H}).

The unit cell of ZrW_2O_8 containing four formula units consists of 44 atoms. There are 132 modes of lattice vibrations. We treat only 3 out of 132 modes as classified acoustic modes. This treatment assumes that only the ''acoustic modes'' within the first Brillouin zone are acoustic modes, while similar modes folded by the zone boundary are classified as ''optical modes.'' The total number of optical modes including such ''optical modes'' is thus 129 per unit cell. The Debye function is assigned to the acoustic modes with the Debye temperature (88.1 K) calculated from the slope of the plot in Fig. 4 assuming three degrees of freedom per 4 f.u. (0.75 degrees of freedom per 1 f.u.). The degrees of freedom assigned to each function and their characteristic temperatures were determined by using a nonlinear least-squares method. Some trials showed that at least two Einstein and two rectangular functions besides one Debye function were necessary for a good fit.

The heat-capacity data from 1.8 to 210 K below the crossing temperature of heat-capacity curves are used for the analysis. For ZrW_2O_8, the contribution of thermal expansion to heat capacity is generally very small. However, the measured C_p data were converted approximately to heat capacities at constant volume (C_v) between 80 and 210 K by using the relation $C_p - C_v = VT\beta^2 B_T$, where V, β, and B_T are molar volume, cubic thermal-expansion coefficient, and isothermal bulk modulus, respectively, and the reported parameters for ZrW_2O_8. The experimental values of V and β of ZrW_2O_8

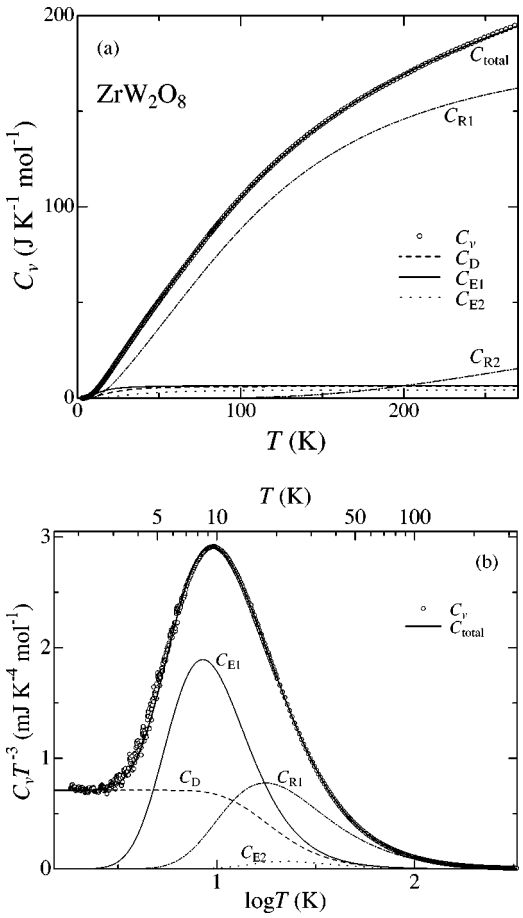

FIG. 6. Heat-capacity contributions of five functions (C_{D}, C_{E1}, C_{E2}, C_{R1}, C_{R2}), the sum of them ($C_{\mathrm{total}} = C_{\mathrm{D}} + C_{\mathrm{E1}} + C_{\mathrm{E2}} + C_{\mathrm{R1}} + C_{\mathrm{R2}}$), and C_v obtained from the experimental heat-capacity data for ZrW_2O_8 in the C-T plot (a) and CT^{-3} vs log T plot (b). In (b), C_{R2} is excluded due to the small contribution to heat capacity.

at various temperatures were taken from Ref. 13. B_T of ZrW_2O_8 is reported to be 72.5 GPa at room temperature (RT) by Jorgensen *et al.*[25] Since $[B_T(100\ \mathrm{K}) - B_T(RT)]/B_T(RT)$ was estimated to be less than 0.5%,[26] it is assumed that B_T is independent of temperature in this study. The difference between C_p and C_v is negligibly small at low temperature (about 0.6% of C_p at 100 K). Thus, C_p was identified as C_v between 1.8 and 80 K without correction.

The result of the fit for ZrW_2O_8 is shown in Fig. 6 as a function of temperature. Each heat-capacity contribution of these five functions (C_{D}, C_{E1}, C_{E2}, C_{R1}, C_{R2}) and the sum of them ($C_{\mathrm{total}} = C_{\mathrm{D}} + C_{\mathrm{E1}} + C_{\mathrm{E2}} + C_{\mathrm{R1}} + C_{\mathrm{R2}}$) are plotted in Fig. 6(a), with the corrected experimental C_v. The total heat capacity C_{total} reproduces the C_v very well. Most parts of the heat capacity below 300 K are attributed to the C_{R1}. The C_{D}, C_{E1}, C_{E2}, C_{R1}, and C_{total} are plotted as CT^{-3} vs log T in Fig. 6(b). It is clear that the maximum peak at about 9.5 K consists of the $C_{\mathrm{E1}}T^{-3}$ and $C_{\mathrm{R1}}T^{-3}$ mainly. The maximum of $C_{\mathrm{E2}}T^{-3}$ is located at about 22 K and overlaps with $C_{\mathrm{R1}}T^{-3}$. Although the fit seems to be given without the E2 mode at first glance, the good fit could not be obtained without the E2 mode. The parameters determined for ZrW_2O_8 are summarized in Table II.

TABLE II. Parameters of each mode obtained from the analysis of heat capacities for ZrW_2O_8 and HfW_2O_8.

Mode	Degrees of freedom	ZrW_2O_8 Θ (K)	ZrW_2O_8 γ_i	HfW_2O_8 Θ (K)	HfW_2O_8 γ_i
D	3 (0.75) [a]	88.1	3.2	87.0	1.4
E1	3.12 (0.78) [a]	41.8	-42	40.8	-40
E2	2.08 (0.52) [a]	111	0.07 [b]	114	0.06 [b]
R1	90 (22.5) [a]	59.6–608		57.9–589	
R2	33.6 (8.4) [a]	831–1747	-0.3	931–1743	-0.2

[a]Degrees of freedom/N_A.
[b]γ_{E2+R1}, see the text.

Figures 7(a) and 7(b) show the effective DOS of ZrW_2O_8, together with the experimental DOS, $g_n(\omega)$, obtained from inelastic neutron scattering.[5] It is not easy to compare the effective DOS with the experimental $g_n(\omega)$, because the $g_n(\omega)$ is a neutron cross-section weighted DOS. It is, however, still possible to compare them at some points. Any phonon modes above 150 meV were not found by the neutron study. The upper limit value agrees very well with the highest characteristic temperature of R2 ($\Theta_{R2H}=1747$ K, 150.5 meV). On the other hand, the lowest limit of the characteristic temperature of all the modes except the Debye mode is E1 ($\Theta_{E1}=41.8$ K, 3.60 meV). The energy of the E1 mode is the same as the peak at the lowest frequency of $g_n(\omega)$.

The effective DOS is divided into two groups, which mainly consist of R1 and R2. There is a wide gap from 610 K (52 meV) to 830 K (72 meV) between R1 and R2. This wide gap is fully consistent with the Raman results as seen in Fig. 3. The experimental $g_n(\omega)$ (Ref. 5) also shows two groups of phonon distribution. The gap exists between 60 and 80 meV as shown in Fig. 7(a), but $g_n(\omega)$ is not completely zero in the gap. The numbers of phonon modes belonging to the low- and high-frequency groups have been reported previously.[24] The low-frequency group has 100 degrees (76%) of freedom: 3 acoustic, 9 lattice, 24 translational, 24 librational, and 40 internal degrees of freedom. On the other hand, the high-energy group has 32 degrees of freedom (24%). Our experimental results in Table II are favorably compared with the reported values. That is, the number of degrees of freedom for our results is about 98.4 (75%) for the low-frequency group (D, E1, E2, R1) and 33.6 (25%) for the high-frequency group (R2).

C. Effective phonon density of states of HfW_2O_8

The deduction of effective phonon DOS applied to ZrW_2O_8 yielded a successful result as shown in a previous section in the comparison with the experimental phonon DOS determined by neutron scattering. The same procedure is then applied to HfW_2O_8. To simplify the comparison with ZrW_2O_8, the number of functions and their degrees of freedom were fixed. Before the fit, a correction of C_p-C_v was made using B_T of HfW_2O_8 (82.0 GPa).[27] The other parameters used for the correction were taken from Ref. 13.

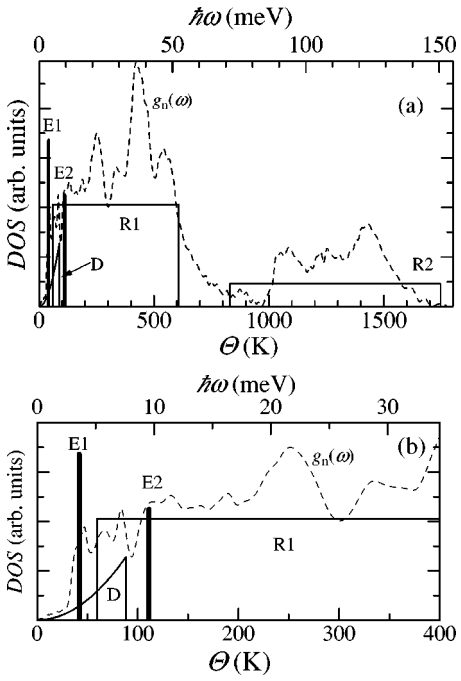

FIG. 7. Calculated effective phonon DOS of ZrW_2O_8 compared with experimental phonon DOS $g_n(\omega)$ obtained from inelastic neutron scattering (Ref. 5). (b) is an enlarged plot of (a).

The parameters determined from the heat-capacity analysis of HfW_2O_8 are given in Table II and the effective DOS of HfW_2O_8 is drawn in Fig. 8(a), together with ZrW_2O_8 for the comparison. Figure 8(a) and Table II show that the highest characteristic temperature (Θ_{R1H}) of the R1 distribution of HfW_2O_8 is slightly lower than that of ZrW_2O_8, whereas the lowest Θ_{R2L} of the R2 distribution of HfW_2O_8 is higher than that of ZrW_2O_8. These changes on going from ZrW_2O_8 to HfW_2O_8 mean the increase of the gap between the R1 and R2 distributions. The increase of the gap and the variation of Θ_{R2L} agree well with the results of the Raman study (see Fig. 3), supporting the fact that the pseudofrequency distribution using rectangular distribution approximates the actual phonon DOS well.

Figure 8(b) shows the total heat capacity ($C_{total}=C_D+C_{E1}+C_{E2}+C_{R1}+C_{R2}$) and each contribution of C_{R1} and C_{R2} for ZrW_2O_8 and HfW_2O_8. The total heat-capacity curves (C_{total}) of ZrW_2O_8 and HfW_2O_8 cross at about 240 K. Figure 8(c) shows the temperature dependence of ΔC_{total}, ΔC_{R1}, and ΔC_{R2} [e.g., $\Delta C_{total}=C_{total}(HfW_2O_8)$-$C_{total}(ZrW_2O_8)$]. ΔC_{total}, shown by a solid line in Fig. 8(c), is quite consistent with ΔC_v, calculated from the experimental results. It is noted that the fits to the corrected heat capacities were done below 210 K, which was lower than the crossing temperature of the heat capacity, 220 K. This again supports the adequacy of the heat-capacity analysis.

D. Comparison of phonon DOS between ZrW_2O_8 and HfW_2O_8 and crossing of heat capacity

We are now ready to compare the effective phonon DOS between ZrW_2O_8 and HfW_2O_8 and to interpret physically

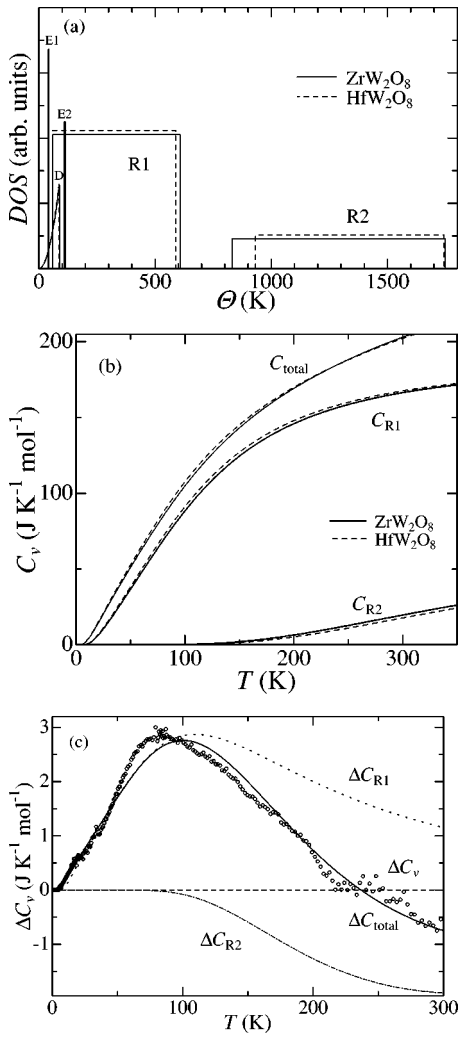

FIG. 8. (a) Calculated effective phonon DOS of ZrW_2O_8 and HfW_2O_8. (b) Total heat capacity ($C_{total}=C_D+C_{E1}+C_{E2}+C_{R1}+C_{R2}$) and heat-capacity contributions of R1 and R2 (C_{R1} and C_{R2}). (c) Temperature dependence of ΔC_{total}, ΔC_{R1}, and ΔC_{R2} [e.g., $\Delta C_{total}=C_{total}(HfW_2O_8)$-$C_{total}(ZrW_2O_8)$].

the origin of the crossing of heat capacity. As seen in Table II, the Θ_{E1} of HfW_2O_8 is lower than that of ZrW_2O_8, so that the E1 mode of HfW_2O_8 is softer than that of ZrW_2O_8. The softening of the E1 mode suggests that the mass effect directly appears here. Figure 9 shows the plots of $C_{E1}T^{-3}$ against $\log T$ for ZrW_2O_8 and HfW_2O_8. It is seen in Fig. 9 that a magnitude of the peak of HfW_2O_8 in the $C_{E1}T^{-3}$ vs $\log T$ plot is larger than that of ZrW_2O_8, in spite of the fact that the same degrees of freedom belong to the E1 mode. Figure 9 shows clearly that the change in the peak of $C_{E1}T^{-3}$ corresponds to the change in the peak of experimental data, on going from ZrW_2O_8 to HfW_2O_8 as seen in Fig. 5. The softening of the E1 mode, therefore, brings about the increase of a magnitude of the peak.

Now, let us discuss the crossing of heat capacity. The contributions of the D, E1, and E2 modes to the heat capacities in Fig. 6(a) are saturated around 100 K. Therefore, those contributions are not involved in the crossing of heat capacity. The C_{R1} makes up the majority of the total heat capacity.

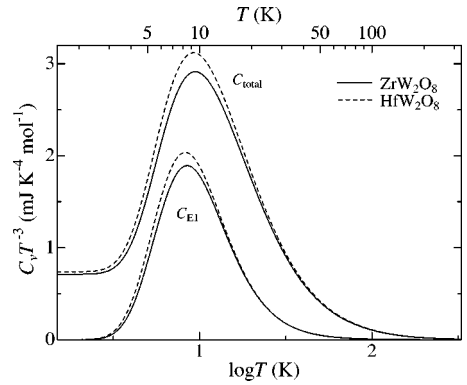

FIG. 9. $C_{total}T^{-3}$ and $C_{E1}T^{-3}$ against $\log T$ for ZrW_2O_8 and HfW_2O_8.

As seen in Fig. 8(c), the ΔC_{R1} is positive [$C_{R1}(HfW_2O_8) > C_{R1}(ZrW_2O_8)$] and more than 1.5 J K^{-1} mol^{-1} at even 250 K. On the other hand, the ΔC_{R2} is negative [$C_{R2}(HfW_2O_8) < C_{R2}(ZrW_2O_8)$] and the absolute value of ΔC_{R2} increases with increasing temperature. Although the heat capacity of HfW_2O_8 is larger than that of ZrW_2O_8 in the low-temperature region, a contribution of C_{R2} to total heat capacity increases with increasing temperature above 100 K, leading to the crossing of heat capacity around 220 K. An important key to account for the temperature dependence of ΔC_{R1} and ΔC_{R2} is the characteristic temperatures Θ_R, since the R1 and R2 distributions of HfW_2O_8 include the same degrees of freedom as those of ZrW_2O_8. HfW_2O_8 and ZrW_2O_8 have nearly the same Θ_{R1L} and Θ_{R2H}, which correspond to the lowest and highest characteristic temperatures of the rectangular distributions, respectively. On the other hand, the Θ_{R1H} of HfW_2O_8 is about 19 K (1.6 meV) lower than ZrW_2O_8, but the Θ_{R2L} is about 100 K (8.6 meV) higher. Thus, a wider gap between two distributions of HfW_2O_8 is seen as shown in Fig. 8(a). The increase of the gap between R1 and R2 distributions causes the different temperature dependencies of ΔC_{R1} and ΔC_{R2}, leading to the crossing of heat capacity between ZrW_2O_8 and HfW_2O_8.

The difference in phonon DOS between ZrW_2O_8 and HfW_2O_8 originates, at least, in two factors: mass and bond strength. The increase in mass from Zr to Hf tends to soften the translational modes. On the other hand, it is hard to imagine the change of the bond strength from chemical intuition. However, we know that the Debye temperature changes less than that expected from the mass effect as described in a previous section. This indicates that the bond strength of HfW_2O_8 is stronger by a factor 1.15 in terms of force constant. The bond strength affects all types of modes. In summary, on going from ZrW_2O_8 to HfW_2O_8, the low-frequency modes involving translational degrees of freedom of MO_6 polyhedra (M=Zr or Hf) soften mainly due to the mass effect, whereas the high-frequency modes which are intrapolyhedra vibrations harden due to the enhancement of bonds strength. The former modes may be expressed as D, E1, and R1 modes in the present analysis of phonon DOS, and the latter is the R2 mode. It was reported that the vibrational modes above 80 meV were the streching modes of WO_4.[2,10,24] If so, it is considered that the vibrational modes

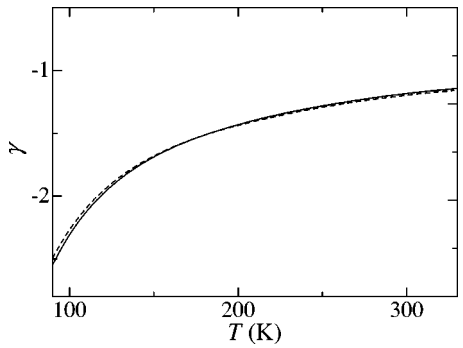

FIG. 10. Temperature dependence of Grüneisen functions of ZrW_2O_8 (solid line) and HfW_2O_8 (broken line).

of WO_4 are affected strongly by the difference in bond strength and/or atomic mass between Zr and Hf atoms, bonding to the oxygen atoms in WO_4.

E. Grüneisen parameter of ZrW_2O_8 and HfW_2O_8

The Grüneisen function γ is defined by the following equation,[28]

$$\gamma(T,V)=\left[\frac{\partial P}{\partial(U/V)}\right]_V, \tag{3}$$

where V is the molar volume, P the pressure, and U the internal energy. γ is related to the cubic thermal-expansion coefficient β, isothermal bulk modulus B_T, heat capacity at constant volume C_v, and molar volume V as follows,[28]

$$\gamma=\frac{\beta B_T V}{C_v}. \tag{4}$$

The Grüneisen function γ is given by a heat-capacity weighted average of mode-Grüneisen parameters γ_i of the ith vibrational mode, i.e.,

$$\gamma=\frac{\sum \gamma_i C_i}{\sum C_i}, \tag{5}$$

where the mode-Grüneisen parameter (γ_i) is defined by the volume dependence of mode frequencies (ν_i),

$$\gamma_i=-\left(\frac{\partial \ln \nu_i}{\partial \ln V}\right). \tag{6}$$

The negative thermal-expansion materials show $\gamma<0$, because $C_v, V, B_T>0$ and $\beta<0$. Modes with $\gamma_i<0$ are therefore closely related to the mechanism of the negative thermal expansion.

Using the experimental V, B_T, β, and C_v, the Grüneisen functions γ of ZrW_2O_8 and HfW_2O_8 are estimated from Eq. (4) as seen in Fig. 10. Both γ are negative and nearly the same absolute values in the temperature region 90–330 K. Although both γ show very similar temperature dependence in this region, the curves of both γ cross around 180 K. The crossing of γ for ZrW_2O_8 and HfW_2O_8 is attributed to that of their heat capacities. Besides, effective ''mode-Grüneisen parameters'' for vibrational modes used in the analysis of heat capacity are also determined from Eq. (5) and the results are as given in Table II. The mode-Grüneisen parameters γ_{E2+R1} were calculated from E2 and R1 modes together, because E2 and R1 modes are the same type of mode inherently and overlap each other at Θ_{E2}. γ_{E1} of ZrW_2O_8 and HfW_2O_8 are estimated to be -42 and -40, respectively, as shown in Table II. Thus, negative and large absolute values of γ_{E1} mean that E1 modes around 3.5 meV (41 K) are closely related to the negative thermal expansion. Those values of γ_{E1} for ZrW_2O_8 and HfW_2O_8 in this study are consistent with the reported values of $\gamma_i=-32.7$ (Ref. 8) and -27.1 (Ref. 6) for ZrW_2O_8.

F. Characterization of E1 and E2 modes

Now we consider the low-frequency modes of ZrW_2O_8 and HfW_2O_8 in some detail. The effective phonon densities of states of ZrW_2O_8 and HfW_2O_8 have two distinct Einstein modes (E1 and E2) in a low-frequency region. The characteristic temperatures of the E1 modes (Θ_{E1}) for ZrW_2O_8 and HfW_2O_8 are determined to be 41.8 K (3.60 meV) and 40.8 K (3.52 meV), respectively. Both E1 modes have a negative mode-Grüneisen parameter as described above.

The characteristic temperatures of the E2 mode (Θ_{E2}) for ZrW_2O_8 and HfW_2O_8 are obtained as 111 K (9.57 meV) and 114 K (9.82 meV), respectively. The Θ_{E2} of HfW_2O_8 is higher than that of ZrW_2O_8 (hardening). The hardening of optical-phonon modes is also seen in Raman results (see Table II). From the hardening of the E2 mode and the magnitude of Θ_{E2}, the E2 mode seems to correspond to the optical-phonon mode at 86.2 cm^{-1} (10.7 meV) for ZrW_2O_8 in Table II. The previous Raman study under pressure[24] demonstrates that the E2 mode has a negative mode-Grüneisen parameter with the largest absolute value ($\gamma_i=-4.66$) (see the fourth column in Table I). It is, thus, expected that this mode is closely connected to the mechanism of the negative thermal expansion.

Previous works (inelastic neutron scattering,[5,6] heat capacity,[7] analysis of thermal expansion,[8,9] and lattice-dynamic calculation[10,11]) have shown that ZrW_2O_8 has a group of vibrational modes in the region between 1.5 and 8.5 meV with large negative mode-Grüneisen parameters. It is suggested that the modes centered at 5 meV correspond to librational and translational modes of undistorted ZrO_6 and WO_4 polyhedra and make up the major contributions to the negative thermal expansion. These modes correspond to the E1 mode obtained in this study. On the contrary, the previous Raman study under pressure[24] has shown that the negative mode-Grüneisen parameters γ_i distribute not only below 8.5 meV but also above 10 meV. In addition, the mode with the largest absolute value of negative γ_i is not at about 5 meV, but at about 86 cm^{-1} (10.7 meV). This mode can be regarded as the E2 mode obtained in this study. It is important to assign the E1 and E2 modes to corresponding lattice vibrations. Before the assignment, we need to take account of the following two points. First, E1 and E2 are optical modes

with low energy, so that the candidates for them are confined to the lattice mode or translational and librational modes of the undistorted polyhedra. Secondly, ZrW_2O_8 and HfW_2O_8 have the differences in both mass and bond length of *M*-O (*M* = Zr, Hf). It is probable that the softening of the E1 mode is attributed to the difference in mass between Zr and Hf atoms. The mass effect often appears in a translational motion of mass point. It is, therefore, expected that the E1 mode originates from the vibrations including the translational motion of the Zr (Hf) atom or undistorted ZrO_6 (HfO_6) octahedron. On the other hand, it is impossible to interpret the hardening of the E2 mode from a standpoint of the mass effect. The bond length of Hf-O is shorter than that of Zr-O, since the ionic radius of Hf^{4+} is smaller than that of Zr^{4+}. Besides, the force constant of HfW_2O_8 is larger than that of ZrW_2O_8 as deduced from the Debye temperature in a previous section. Both facts surely harden the vibrational mode involving no translation of *M* ions for HfW_2O_8. The issue of the vibration of WO_4 is left for further studies.

V. CONCLUSION

The heat capacities and Raman spectra of ZrW_2O_8 and HfW_2O_8 were measured. It was found that the heat capacity of HfW_2O_8 is larger than that of ZrW_2O_8 at very low temperature due to atomic mass effect, but the heat-capacity curves of two compounds cross at about 220 K. The heat-capacity analysis shows that the crossing of two heat-capacity curves is attributable to the increase of the gap between the low- and high-frequency groups in phonon DOS, on going from ZrW_2O_8 to HfW_2O_8. This increase of gap is consistent with the Raman results. The Raman results and the mode-Grüneisen parameters for the effective phonon DOS indicate that the low-energy Einstein modes show large negative mode-Grüneisen parameters. These Einstein modes are closely related to the negative thermal expansion.

*Author to whom correspondence should be addressed. Fax: +81-761-51-1149. Electronic address: +tsuji\@jaist.ac.jp

†Present address: Institute for Materials Research Tohoku University, 2-1-1, Katahira, Aoba-ku, Sendai 980-8577, Japan.

[1] T. A. Mary, J. S. O. Evans, T. Vogt, and A. W. Sleight, Science **272**, 90 (1996).

[2] J. S. O. Evans, T. A. Mary, T. Vogt, M. A. Subramanian, and A. W. Sleight, Chem. Mater. **8**, 2809 (1996).

[3] J. S. O. Evans, W. I. F. David, and A. W. Sleight, Acta Crystallogr., Sect. B: Struct. Sci. **55**, 333 (1999).

[4] J. S. O. Evans, J. Chem. Soc. Dalton Trans. **1999**, 3317 (1999).

[5] G. Ernst, C. Broholm, G. R. Kowach, and A. P. Ramirez, Nature (London) **396**, 147 (1998).

[6] R. Mittal, S. L. Chaplot, H. Schober, and T. A. Mary, Phys. Rev. Lett. **86**, 4692 (2001).

[7] A. P. Ramirez and G. R. Kowach, Phys. Rev. Lett. **80**, 4903 (1998).

[8] W. I. F. David, J. S. O. Evans, and A. W. Sleight, Europhys. Lett. **46**, 661 (1999).

[9] K. Wang and R. R. Reeber, Appl. Phys. Lett. **76**, 2203 (2000).

[10] R. Mittal and S. L. Chaplot, Phys. Rev. B **60**, 7234 (1999); Solid State Commun. **115**, 319 (2000).

[11] A. K. A. Pryde, K. D. Hammonds, M. T. Dove, V. Heine, J. D. Gale, and M. C. Warren, J. Phys.: Condens. Matter **8**, 10 973 (1996); A. K. A. Pryde, M. T. Dove, and V. Heine, *ibid.* **10**, 8417 (1998).

[12] A. W. Slight, T. A. Mary, and J. S. O. Evans, U.S. Patent No. 5514360 (1995).

[13] Y. Yamamura, N. Nakajima, and T. Tsuji, Phys. Rev. B **64**, 184109 (2001).

[14] R. B. Heslop and K. Jones, *Inorganic Chemistry* (Elsevier, Amsterdam, 1976).

[15] R. D. Shannon, Acta Crystallogr., Sect. A: Cryst. Phys., Diffr., Theor. Gen. Crystallogr. **32**, 751 (1976).

[16] K. Eucken, *Landolt-Börnstein, Zahlenwerte und Funktionen aus Physik, Chemie, Astronomie, Geophysik, und Technik*, 6Aufl., II Band, 4 Teil (Springer-Verlag, Berlin, 1961).

[17] Y. Yamamura, N. Nakajima, T. Tsuji, Y. Iwasa, K. Saito, and M. Sorai, Solid State Commun. **121**, 213 (2002).

[18] Y. Yamamura, N. Nakajima, and T. Tsuji, Solid State Commun. **114**, 453 (2000).

[19] A. Junod, T. Jarlborg, and J. Muller, Phys. Rev. B **27**, 1568 (1983).

[20] A. P. Ramirez, B. Batlogg, G. Aeppli, R. J. Cava, E. Rietman, A. Goldman, and G. Shirane, Phys. Rev. B **35**, 8833 (1987).

[21] A. Bernasconi, T. Sleator, D. Posselt, J. K. Kjems, and H. R. Ott, Phys. Rev. B **45**, 10 363 (1992).

[22] W. P. Beyermann, M. F. Hundley, J. D. Thompson, F. N. Diedrich, and G. Grüner, Phys. Rev. Lett. **68**, 2046 (1992).

[23] Y. Yamamura, K. Saito, H. Saitoh H. Matsuyama, K. Kikuchi, and I. Ikemoto, J. Phys. Chem. Solids **56**, 107 (1995).

[24] T. R. Ravindran, A. K. Arora, and T. A. Mary, Phys. Rev. Lett. **84**, 3879 (2000).

[25] J. D. Jorgensen, Z. Hu, S. Teslic, D. N. Argyriou, S. Short, J. S. O. Evans, and A. W. Sleight, Phys. Rev. B **59**, 215 (1999).

[26] O. Kamigaito and N. Kamiya, *Physics of Ceramics* (Uchida Rokakuho, Tokyo, 1998).

[27] J. D. Jorgensen, Z. Hu, S. Short, A. W. Sleight, and J. S. O. Evans, J. Appl. Phys. **89**, 3184 (2001).

[28] T. H. K. Barron and G. K. White, *Heat Capacity and Thermal Expansion at Low Temperatures* (Kluwer Academic, New York, 1999); T. H. K. Barron, J. G. Collins, and G. K. White, Adv. Phys. **29**, 609 (1980).